Effect of NiAl2O4 Formation on Ni/Al2O3 Stability during Dry Reforming of Methane

Effect of $NiAl_2O_4$ formation on Ni/Al_2O_3 Stability during Dry Reforming of Methane

Lu Zhou, [a] Lidong Li,[a] Nini Wei, [b]Jun Li,[b]Kazuhiro Takanabe, [a]and Jean-Marie Basset*[a]

A series of alumina-supported Ni catalysts were prepared to examine their activity and carbon deposition during dry reforming of methane (DRM). By increasing the final calcination temperature to 900°C to form exclusively $NiAl_2O_4$, a catalyst with strong metal–support interactions was obtained. During a long-term DRM reaction (of about 100 h) at 700°C and with CH_4/CO_2 = 1:1, reduced Ni (from $NiAl_2O_4$) showed a high resistance to sintering and coking. The DRM kinetics behaviours of the catalysts calcined at different temperature were also investigated. Carbon growth models were proposed to rationalize the different carbon morphologies observed on the catalysts.

Introduction

Dry reforming of methane (DRM)(Eq. (1)) has become an important research topic over recent years.[1-2] This process uses both greenhouse gases CO_2 and CH_4 to produce syngas H_2/CO at a low ratio of ~1:1 that is a suitable feedstock in Fischer–Tropsch synthesis.

$$CH_4 + CO_2 \leftrightarrow 2CO + 2H_2,\ \Delta H_{298} = +247\ \text{kJ/mol} \quad (1)$$

Numerous supported "monometallic" catalysts have been studied for DRM; more specifically, noble metals based catalysts such as Rh, Ru and Pt are known to exhibit promising performance.[3] However, considering the high cost and the limited availability of noble metals, Ni-based catalysts are more attractive for industrial applications. As for the support, Wang and Lu[4] reported that the use of Al_2O_3 as support for Ni catalysts resulted in a supported Ni catalyst with superior initial activities over Ni catalysts than that used SiO_2, TiO_2, MgO, ZrO_2, CeO_2, La_2O_3, clay, or zeolites as a support. Therefore, Ni/Al_2O_3 catalysts are the most commonly reported DRM catalysts system in the literature.

Nevertheless, it must be pointed out that owing to carbon deposition accompanied with Ni oxidation and/or sintering, Ni/Al_2O_3 catalysts suffer from severe deactivation.

Regarding carbon deposition on Ni/Al_2O_3 catalysts during DRM, it is reported that the mechanism of coke formation is similar to that of steam reforming of methane (SRM).[5] However, the potential for coke formation on Ni catalysts during DRM is much higher. Methane cracking (Eq. (2)) and the Boudouard reaction (Eq. (3)) are believed to be the two main routes of carbon formation.

$$CH_4 \leftrightarrow C + 2H_2,\ \Delta H_{298} = +74.9\ \text{kJ/mol} \quad (2)$$
$$2CO \leftrightarrow CO_2 + C,\ \Delta H_{298} = -172.5\ \text{kJ/mol} \quad (3)$$

[a] Dr. L. Zhou, Dr. L. Li, Prof. K. Takanabe, Prof. J.-M. Basset
KAUST Catalysis Center (KCC)
King Abdullah University of Science and Technology
Thuwal 23955-6900(Saudi Arabia)
Email: jeanmarie.basset@kaust.edu.sa
[b] N. Wei, J. Li
Core Lab
King Abdullah University of Science and Technology
Thuwal 23955-6900(Saudi Arabia)

Wang and Lu [4] reported a coke deposit of 62.76 wt.% on 12 wt.% Ni/Al_2O_3 after 2 h DRM at 700°C; the reaction conditions were CH_4/CO_2 = 1:1, pressure = 1 atm, F/W = 18000 mL/h·$g_{catalyst}$. De Miguel *et al.*[6] reported a coke deposit of 22 wt.% on 10 wt.% Ni/Al_2O_3 after 108 h DRM at 750°C; the reaction conditions were CH_4/CO_2 = 1:1, pressure = 1 atm, F/W = 7000 mL/h·$g_{catalyst}$. As demonstrated in the literature,[7] by adjusting the reaction conditions, thermal dynamical coking can be inhibited and Ni/Al_2O_3 catalysts can thus maintain their activity. Xu *et al.*[8] reported a 120-h stable DRM activity over a 9.17 wt.% Ni/Al_2O_3 catalyst at 700°C, with a CO_2/CH_4 ratio of 1.3:1. Gadalla *et al.*[9] and many other researchers also suggested that higher CO_2/CH_4 ratios could suppress coke deposition on Ni/Al_2O_3 catalysts. However, for industrial processes, a ~1:1 CO_2/CH_4 ratio is preferred. Higher CO_2/CH_4 ratios could improve the reverse water–gas shift (RWGS) reaction (Eq. (4)), thus resulting in lower H_2 selectivity. Furthermore, methane sources, such as biogas, usually comprise CO_2/CH_4 ratios of less than one.

$$CO_2 + H_2 \leftrightarrow CO + H_2O,\ \Delta H_{298} = +46.1\ \text{kJ/mol} \quad (4)$$

Based on the above discussion, a catalyst that kinetically inhibits carbon formation under conditions that are thermodynamically favourable for carbon deposition is urgently required for the DRM process. Therefore, the investigation of coking-resistant Al_2O_3-supported Ni catalysts has become a very important subject and much effort has recently been devoted to the design of coking-resistant Ni/Al_2O_3-based catalysts by decorating the Ni particles with trace amounts of noble metals.[10] In our previous research,[11] we also reported a good DRM stability over Ni/Pt bimetallic catalysts. Nevertheless, it is obvious that these noble metal decorated catalysts are unsuitable on a commercial scale because of their high cost.

The formation of $NiAl_2O_4$ spinel has generally been considered to be another route leading to the deactivation of Ni/Al_2O_3 catalysts during methane reforming reactions.[3, 9] $NiAl_2O_4$ can easily form under reaction between Ni and Al_2O_3; however, it is believed that the $NiAl_2O_4$ spinel cannot be easily reduced to $Ni^{(0)}$ and thus its formation should lower the amount of active Ni. Only limited literature reports demonstrate the positive influence of $NiAl_2O_4$ on catalyst activity. Alternatively, Enger *et al.*[12] recently reported that reducing the $NiAl_2O_4$ at 800°C to nano-sized (15–25 nm) Ni particles afforded a catalyst with good SRM activity. Ribeiro *et al.*[13] prepared a $NiAl_2O_4$ catalyst with a high surface

area that was activated with CH_4/O_2. The resulting catalyst displayed excellent DRM stability for more than 40 h. In our recent study,[14] we reported the excellent SRM activity of a plate-type anodic alumina-supported Ni catalyst featuring an interfacial $NiAl_2O_4$ layer; moreover, coke deposition was suppressed and the Ni particle sintering rate was reduced. The catalyst was examined in DRM, and showed good initial activity. Chen and Ren[15] studied the influence of calcination temperature on the activity of a 13 wt.% Ni/Al_2O_3 catalyst for DRM. They concluded that the formation of $NiAl_2O_4$ suppressed coke deposition. However, the DRM process was only conducted over a relatively short period of 3 h at 750°C, and the applied CH_4/CO_2 ratio of 1:2 was above the normal industrial requirement.

As a consequence of these preliminary published results, we investigated in detail, in the present work, the effect of $NiAl_2O_4$ formation on the Ni/Al_2O_3 catalyst performance during a long-term DRM process (of about 100 h) at 700°C and with a CH_4/CO_2 of 1:1. The aim was to develop a relatively cheap catalyst without any added promoters. The catalyst structure, catalyst reducibility, and Ni particle dispersion, size, morphology and amount of deposited carbon were characterized with X-ray diffraction (XRD), thermo gravimetric analysis (TGA), transmission electron microscopy (TEM), temperature-programmed reduction (TPR), and temperature-programmed desorption (TPD). The DRM and carbon formation kinetic behaviours of the catalysts are also reported.

Results and Discussion

Influence of $NiAl_2O_4$ formation on catalysts structure

The XRD patterns of the as-prepared catalysts, calcined at different temperatures, are shown in Figure 1 (patterns a–c). With increasing calcination temperatures, the Al_2O_3-supported Ni catalysts exhibited stronger $NiAl_2O_4$ but weaker NiO diffraction peaks. It is well known that under a high-temperature calcination condition, nickel ions have sufficient energy to overcome the surface barrier of alumina and integrate into the alumina lattice to form the spinel structure, i.e., NiO reacts with Al_2O_3 to form $NiAl_2O_4$. This is evident from the XRD results that show that high temperatures, such as 900°C, favour such reaction; the sample $Ni/Al_2O_{3(900)}$ that was calcined at 900°C displayed only $NiAl_2O_4$ peaks as Ni-oxides.

Stating that in the DRM the metallic state of Ni is required, a pre-reduction of the catalyst is in principle needed. Figure 2 shows the reducibility performance of different catalysts by H_2-TPR analysis.

The TPR results confirmed the existence of different types of nickel oxides present in the *as-prepared* catalysts. According to our previous report,[14] the reduction peaks observed below 600°C can be ascribed to the reduction of NiO to Ni(0) nanoparticles, whereas the peaks observed between 600 and 800°C can be ascribed to the reduction of "$NiO{\cdot}Al_2O_3$" (or better described as surface $NiAl_2O_4$). The peaks observed above

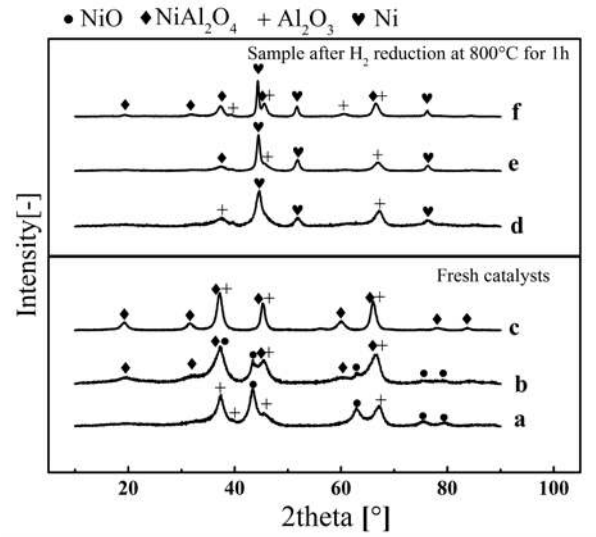

Figure 1. XRD patterns over different samples. a) fresh $Ni/Al_2O_{3(350)}$, b) fresh $Ni/Al_2O_{3(700)}$, c) fresh $Ni/Al_2O_{3(900)}$, d) reduced sample a, e) reduced sample b, f) reduced sample c.

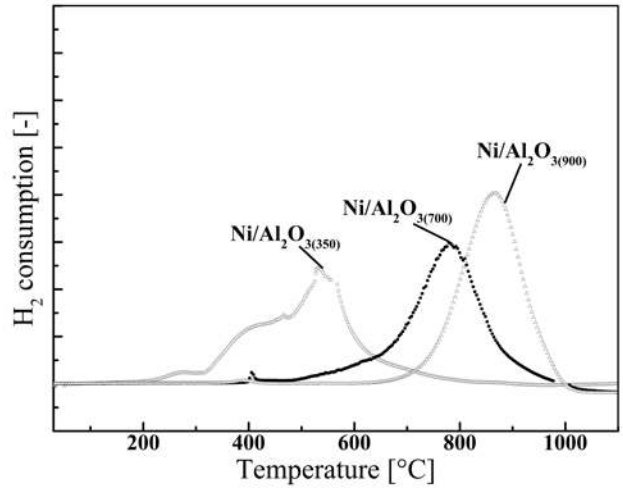

Figure 2. H_2-TPR of fresh catalyst.

800°C were attributed to the reduction of crystalline spinel $NiAl_2O_4$ to Ni(0) nanoparticles Consequently, it can be concluded that $Ni/Al_2O_{3(350)}$ mainly consists of NiO, $Ni/Al_2O_{3(700)}$ consists of $NiO{\cdot}Al_2O_3$, and $Ni/Al_2O_{3(900)}$ consists of $NiAl_2O_4$ only.

In this study, the catalysts pre-reduction was performed with pure H_2 at 800°C. The reduction degree was calculated by the TPR profiles done at 800°C, while assuming that the Ni exists as Ni^{2+}. The calculated results showed that, following H_2 reduction at 800°C, $Ni/Al_2O_{3(350)}$ primarily featured metallic Ni (also see Figure 1 pattern d), whereas 61% and 7% of the nickel oxide in $Ni/Al_2O_{3(700)}$ and $Ni/Al_2O_{3(900)}$, respectively, were reduced to metallic Ni. Because the nickel oxides in $Ni/Al_2O_{3(700)}$ and $Ni/Al_2O_{3(900)}$ could not be completely reduced at the selected

Table 1. Change of catalysts structure properties with different pre-reduction

Samples	Ni particle size [nm][a]		Ni crystallite size [nm][b]	
	800°C reduction	1100°C reduction	800°C reduction	1100°C reduction
$Ni/Al_2O_{3(350)}$	9.34	32.38	9.23	31.97
$Ni/Al_2O_{3(700)}$	11.47	29.34	10.67	27.78
$Ni/Al_2O_{3(900)}$	12.86	20.93	11.65	19.87

[a] Particle size detected by TEM
[b] Crystallite size calculated from Sherrer equation

Table 2. Characterization of catalysts in this study

Samples	Ni loading [wt%]	BET area [m^2/g]	Pore volume [cc/g]	Dispersion[a] [%]
$Ni/Al_2O_{3(350)}$	16.35	91.66	0.151	9.31
$Ni/Al_2O_{3(700)}$	16.26	81.14	0.154	8.17
$Ni/Al_2O_{3(900)}$	16.32	57.48	0.151	7.49
Alu130		133.56	0.365	

[a] Catalysts reduced by H_2 at 800°C for 1h

temperature (i.e., 800°C), the resulting two catalysts are best referred to as Ni-$NiAl_2O_4$–Al_2O_3. These were confirmed by the XRD patterns of the catalysts that underwent H_2 reduction at 800°C. As observed in Figure 1 (patterns e–f), the co-existence of Ni and $NiAl_2O_4$ were observed for $Ni/Al_2O_{3(700)}$ and $Ni/Al_2O_{3(900)}$.

The Ni metal morphology and size distribution of the reduced catalysts were investigated by TEM (Figure 3). The average particle size of metallic Ni measured by TEM on each sample is listed in Table 1. According to the TPR profiles in Figure 2, the reduction temperature of 800°C is too low to reduce the $NiAl_2O_4$. Perhaps this is the reason why, among these reduced catalysts (Figure 3a-c), little difference on the particle size can be seen. The $Ni/Al_2O_{3(350)}$ shows the smallest mean Ni particle size of 9 nm. The $Ni/Al_2O_{3(900)}$ shows the largest mean particle size of around 13 nm.

Therefore, the influence of different nickel oxides supported on alumina, especially $NiAl_2O_4$, on Ni sintering was investigated by assessing the change in Ni size would follow reduction of the catalysts under pure H_2 at a relatively high temperature of 1100°C for 1 h. As observed in Figure 3A-C, the presence of $NiAl_2O_4$ exerted a positive effect on Ni sintering. The particle size decreases from 32 nm for $Ni/Al_2O_{3(350)}$ to 29 nm for $Ni/Al_2O_{3(700)}$ and to only 21 nm for $Ni/Al_2O_{3(900)}$. Considering the different Ni-oxides over these samples, it is reasonable to conclude that the $NiAl_2O_4$ existence helps to stabilize the Ni particles toward sintering under high reaction temperature. And this stabilizing effect of nickel aluminate was most likely because of a stronger nickel bonding to nickel aluminate relative to that with the alumina. The nickel aluminate, in turn, bonded well to alumina, and the nickel aluminate was effectively incorporated into the surface of the alumina support.[16] It is likely that

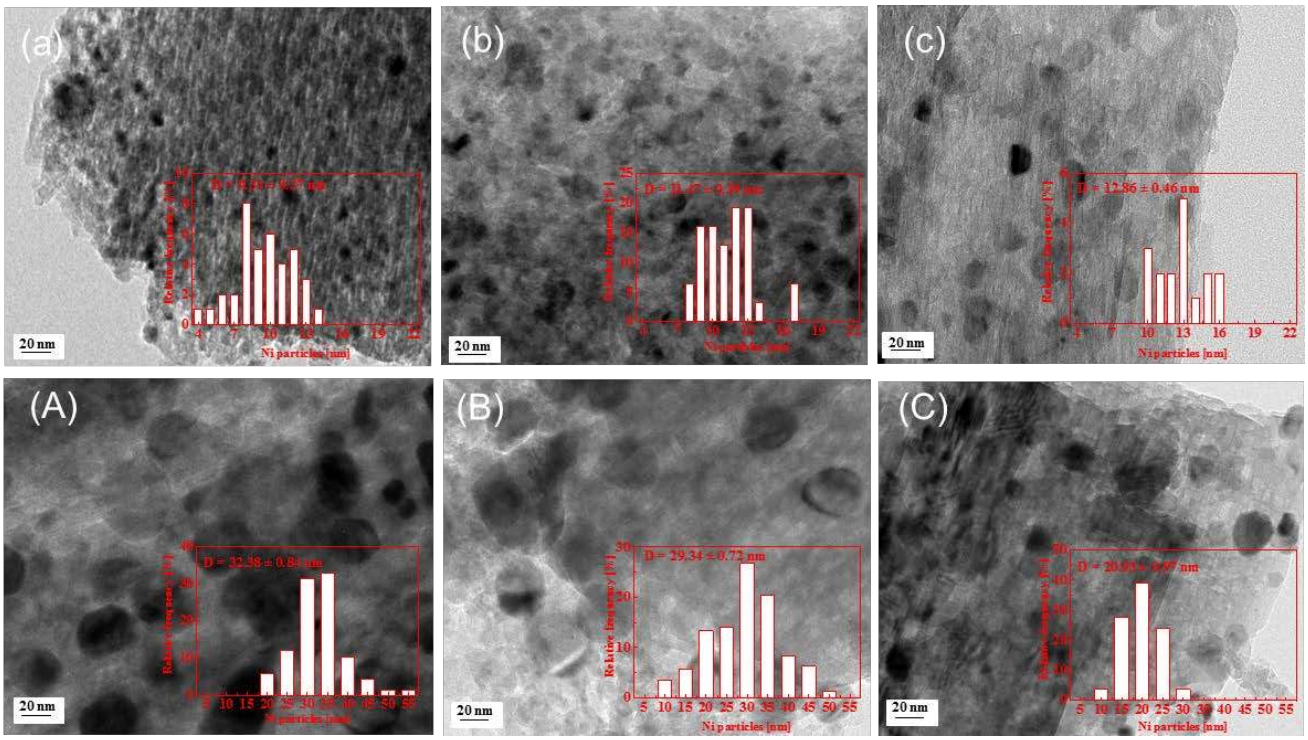

Figure 3. TEM images of H_2 reduced samples. After reduction at 800°C for 1h: (a) $Ni/Al_2O_{3(350)}$, (b) $Ni/Al_2O_{3(700)}$, (c) $Ni/Al_2O_{3(900)}$; After reduction at 1100°C for 1h: (A) $Ni/Al_2O_{3(350)}$, (B) $Ni/Al_2O_{3(700)}$, (C) $Ni/Al_2O_{3(900)}$.

incomplete reduction of $NiAl_2O_4$ produces Ni sites that can strongly interact with a $Ni_xAl_yO_z$ support. The $Ni_xAl_yO_z$ support can be considered as a deficient $NiO–Al_2O_3$ solid solution-like species featuring a number of Ni^{2+} defects. It is proposed that such defects play an important role in stabilizing the catalytic size of Ni.

The Ni loading in Table 2 was ~16 wt.%. Because of the alumina support sintering under increasing calcination temperatures, the BET areas decreased in the order of $Ni/Al_2O_{3(350)}$ > $Ni/Al_2O_{3(700)}$ > $Ni/Al_2O_{3(900)}$. The dispersion was consistent with the Ni particle size in Table 1.

Kinetic investigation of the DRM catalytic activity

The effect of temperature (500–800°C) on the reaction rates of methane and CO_2 consumption and product formation (CO and H_2) over the three types of *as-prepared* alumina-supported Ni catalysts was investigated. For each temperature case studied, the reaction rates were calculated from the initial reaction stage (20 min) to ensure precise control of catalytic activity of the preformed catalyst. The TOF for the reactants CH_4 and CO_2 and the product H_2/CO ratio as a function of temperature are presented in Figure 4. It is obvious that both CH_4 and CO_2 conversions and H_2/CO ratio increased with increasing temperatures regardless of the catalyst studied. The H_2/CO ratio determined at 500°C was only 0.45 and increased to 0.7 at 800°C. These values were far away from the values predicted from the thermodynamic calculations. At low temperatures (500–600°C), all catalysts exhibited similar activity in terms of CH_4 and CO_2 conversion and H_2/CO ratio, whereas at high temperatures (650–800°C), the activity increased in the order of $Ni/Al_2O_{3(900)}$ < $Ni/Al_2O_{3(700)}$ < $Ni/Al_2O_{3(350)}$. The difference in the initial TOF activities among these three samples may be related to the size of the Ni particles. Similar results were reported by Wang *et al.*[17] who prepared a series of NiO/MgO catalysts with different Ni particle sizes (3–20 nm) and observed that the activity, as measured by CH_4 TOF, increased with reducing Ni particle sizes. They suggested that the coordinatively unsaturated surface atoms prevails in small crystallites and are significantly more active than those in the low-index planes predominately exposed on large crystallites.

The apparent activation energies calculated from the Arrhenius plots are shown in Figure 5. Regardless of catalyst studied, the activation energy for CH_4 consumption was in agreement with that reported by Osaki *et al.*[18] (i.e., ~33 kJ/mol). The activation energy of CO_2 consumption was higher than that of CH_4 consumption, indicating that the activation of CO_2 is more temperature sensitive than that of methane. Lower CO_2 activation energies (relative to those of CH_4) are usually reported for catalyst supports with a strong Lewis base character such as MgO, ZrO_2, and TiO_2. Guo *et al.*[19] reported CH_4 and CO_2 activation energies of 26.39 and 40.43 kJ/mol, respectively, over 5% $Ni/MgAl_2O_4$, consistent with the findings of the present study. Both CH_4 and CO_2 activation energies were lower than those for CO and H_2 production, suggesting that the rate-determining steps for CO and H_2 formation are different from those for CH_4 and CO_2 consumption. The activation energy for H_2 production is

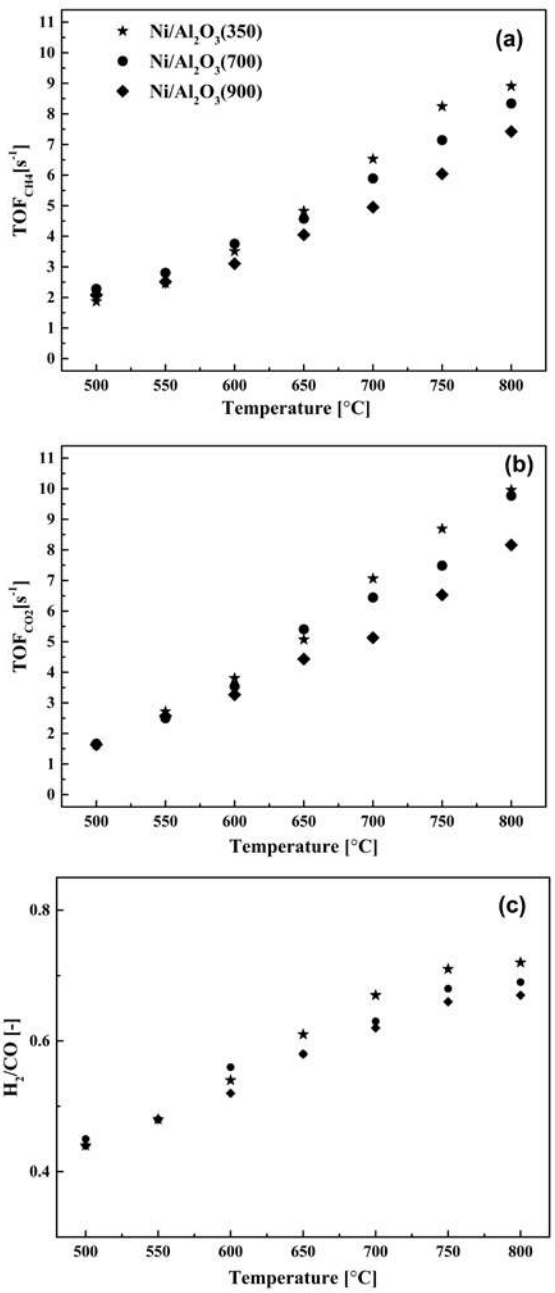

Figure 4. Reaction rates as a function of temperature and H_2/CO ratio over different catalysts at N_2:CH_4:CO_2 = 2:1:1, F/W = 480 L/g_{cat}·h, 700°C: (a) CH_4 TOF; (b) CO_2 TOF; (c) H_2/CO ratio.

significantly higher than that for CO, thereby indicating that the RWGS reaction (which consumes H_2 and produces CO) strongly influences the formation of H_2, thus generating an H_2/CO ratio of less than 1(Figure 4c). It has been reported that supports can significantly influence the activation energy by altering the rate-controlling step in the reaction sequence.[20] The difference in the activation energies of these three catalysts is thus most likely because of the different support composition. A higher amount of non-reduced $NiAl_2O_4$ will remain supported on the alumina support and act as the "real" support for catalysts

Table 3. Catalysts stability performance at N_2:CH_4:CO_2 = 2:1:1, F/W = 480 L/g_{cat}·h, 700°C.

Samples	TOF_{CH4} [s^{-1}]				Coking amount [wt%][a]
	0.5h	15h	40h	100h	
$Ni/Al_2O_{3(350)}$	6.5	3.2	2.6	1.7	36.97
$Ni/Al_2O_{3(700)}$	5.9	3.6	3.2	2.9	16.33
$Ni/Al_2O_{3(900)}$	5.1	4.5	4.4	4.4	7.93

[a] coking amount was calculated by TGA over catalysts after 100 h DRM in Figure 6.

prepared at higher calcination temperatures, thereby altering the surface mechanism.

Table 3 presents the catalytic DRM stability performance over the three types of catalysts prepared in this study. Catalysts prepared at higher calcination temperatures showed better stability. Both $Ni/Al_2O_{3(350)}$ and $Ni/Al_2O_{3(700)}$ suffered severe deactivation within the early stages of the process. $Ni/Al_2O_{3(350)}$ catalyst showed a 50% loss of its initial activity within the first 15 h of reaction and only retained 30% of its initial activity after 100 h of reaction, whereas Ni/Al_2O_3(700) lost 40% of its initial activity within the first 15 h of reaction and retained almost 50% of its initial activity after 100 h of reaction. $Ni/Al_2O_{3(900)}$ only lost 10% of its initial activity within the first 15 h of reaction, and negligible catalyst deactivation was evidenced within the remaining 85 h of reaction, which we consider as a remarkable result. The coking amount of the three catalysts after 100 h DRM, as shown in Table 3, clearly demonstrating that the $NiAl_2O_4$ reduced the extent of carbon deposition on the reduced catalyst. The "Ni" from the reduction of $NiAl_2O_4$ over $Ni/Al_2O_{3(900)}$ resulted in only a 8-wt.% coking, whereas the "Ni" from the reduction of NiO over $Ni/Al_2O_{3(350)}$ resulted in a 37-wt.% coking after 100 h DRM. The "Ni" from reduced $Ni/Al_2O_{3(700)}$ comprising both $NiO·Al_2O_3$ and $NiAl_2O_4$ resulted in moderate 16-wt.% coking.

Small Ni particles are often reported to limit the level of coking during DRM. Hu and Ruckenstein[21] concluded that large Ni particles stimulate carbon deposition. However, according to the present data (Table 1) it could be seen that the Ni particle size

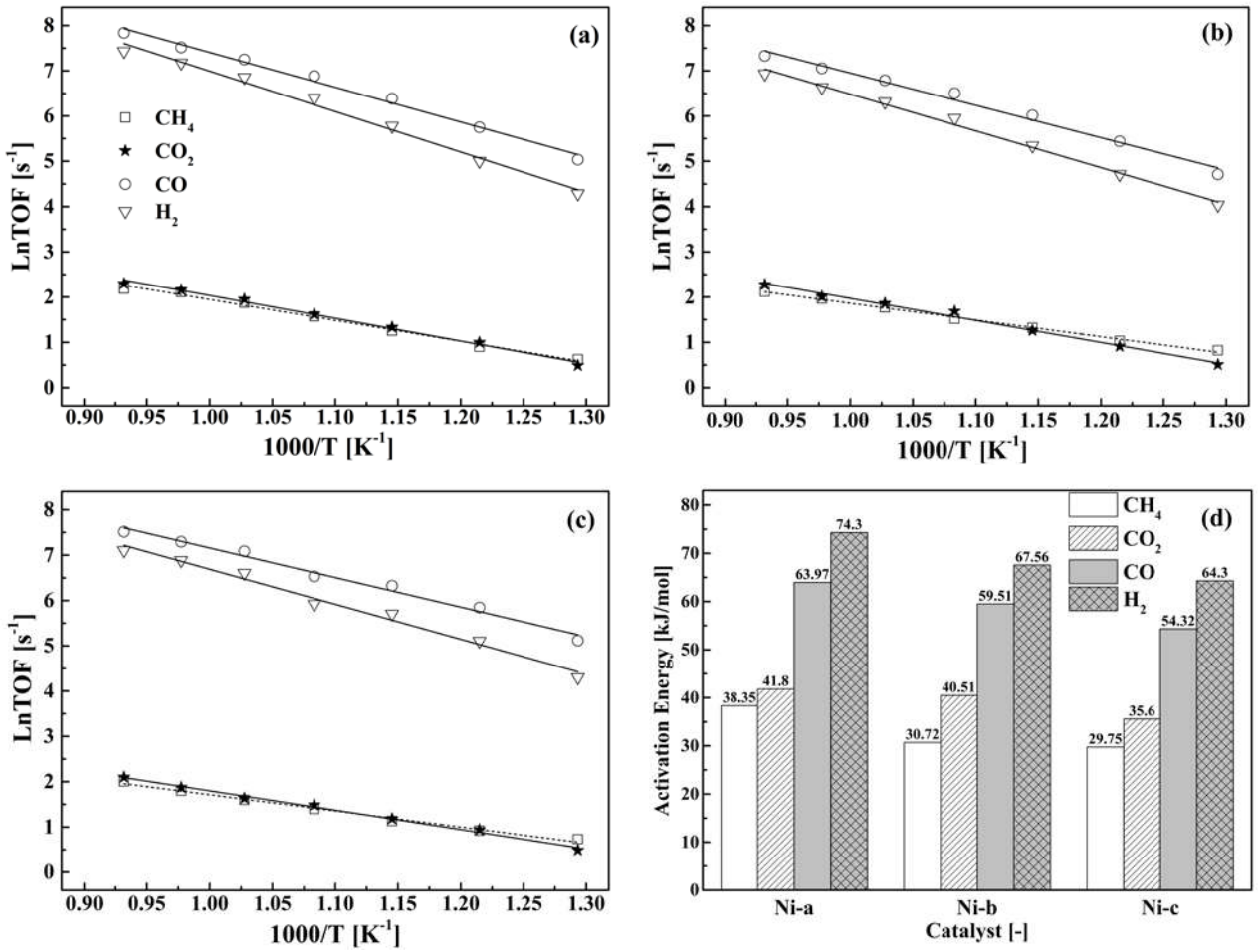

Figure 5. Arrhenius plots and apparent activation energies over different catalysts at N_2:CH_4:CO_2 = 2:1:1, F/W = 480 L/g_{cat}·h: (a) $Ni/Al_2O_{3(350)}$; (b) $Ni/Al_2O_{3(700)}$; (c) $Ni/Al_2O_{3(900)}$; (d) Apparent activation energies.

was not the only factor influencing carbon deposition. Although the Ni particles sizes of three reduced samples were similar, the level of coke deposition was totally different. These results indicate that in addition to the Ni particle size, the physicochemical state of the nickel oxide species in the as-prepared catalyst sample influenced carbon deposition. Juan-Juan *et al.*[22] indicated that besides the particle size, other factors, such as particle morphology or structure, influence carbon deposition. It is reasonable to conclude that the "Ni" from the reduction of $NiAl_2O_4$ would suppress coking to a higher degree than that the "Ni" from NiO and/or $NiO{\cdot}Al_2O_3$ during DRM. NiO species that are prone to reduction would produce Ni sites with weak metal–support interactions, which could be responsible for the severe sintering and coking observed for $Ni/Al_2O_{3(350)}$ and $Ni/Al_2O_{3(700)}$. The Ni particles reduced in $Ni/Al_2O_{3(900)}$, i.e., partial reductive extraction of Ni^{2+} ions from $NiAl_2O_4$, are expected to adequately strongly interact with the support to inhibit carbon deposition. Enger *et al.*[12] reported that the reduction of $NiAl_2O_4$ does not simply yield Ni/Al_2O_3, but bimetallic species such as $NiAl_x/Al_zO_y$. Considering that in a reducing atmosphere Ni from $NiAl_2O_4$ forms such kind of a defective $Ni_xAl_yO_z$ phase, which has probably a higher oxygen surface mobility, the high stability of the samples containing $NiAl_2O_4$ can be also related to a higher rate of carbon gasification over these samples.

Carbon deposition on different catalysts

Figure 6 shows the TGA–DTA data for the spent catalysts after undergoing 100 h DRM. As noted, an increase in the sample weight was observed at temperatures of 300–430°C that could be due to the oxidation of Ni to nickel oxides. The amount of deposited coke on the different catalysts was calculated based on the TGA curves and the results are shown in Table 3. Oxidation of carbonaceous deposit with oxygen in air is an exothermic process, and DTA was employed to investigate the decoking of catalysts. All three spent samples displayed two distinct exothermic peaks at 500–550°C and 680–700°C. This indicates the deposit of more than one type of carbon species on the catalyst surface. According to the literature,[23] deposited carbon on Ni-based catalyst surfaces can be classified into three types: amorphous carbon C_α, filament carbon C_β, and graphite carbon C_γ. Deposited C_α is often reported to be an active carbon species during DRM and can easily be eliminated by oxidation or H_2-reduction at temperatures as low as 250–350°C. Some researchers[24] explain that C_α originates from nickel carbide that is produced during methane decomposition and does not affect the catalyst DRM activity. C_γ is an inert carbon species and requires temperatures higher than 600°C for removal. C_β is known to possess a relatively high activity and can be eliminated at a relatively low temperature. Therefore, the DTA peak observed at 680–700°C could be ascribed to the oxidation of graphite carbon C_γ, whereas the peak at 500–550°C can be attributed to filament carbon C_β. XRD patterns of the spent catalysts following 100 h DRM, shown in Figure 7, also demonstrate the existence of graphitic carbon in all three samples; the intensity of graphite carbon in spent $Ni/Al_2O_{3(900)}$ was the lowest. The DTA result also showed that the intensity of the C_γ peak decreased in the order of $Ni/Al_2O_{3(350)}$ > $Ni/Al_2O_{3(700)}$ > $Ni/Al_2O_{3(900)}$. These findings support the different DRM stability observed in Table 3. As reported,[24] C_α and C_β can gradually

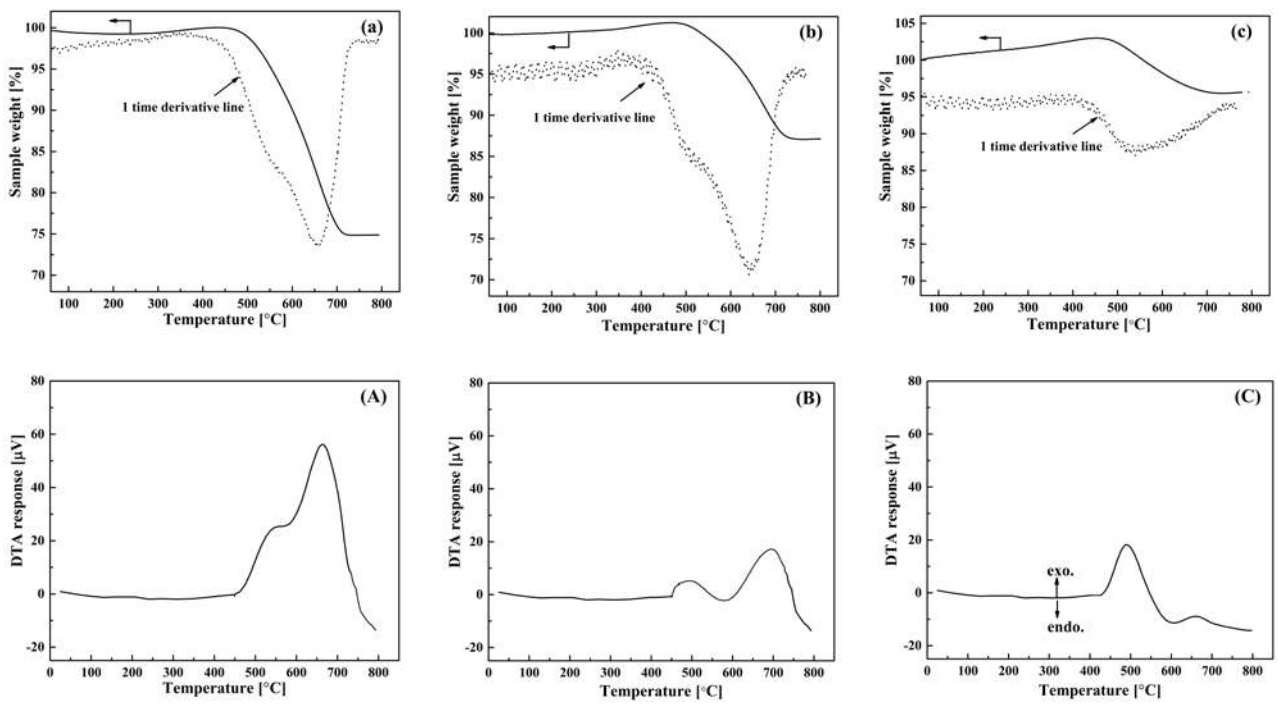

Figure 6. TGA-DTA behaviour of different catalysts after DRM in Table 3: (a)(A) $Ni/Al_2O_{3(350)}$; (b)(B) $Ni/Al_2O_{3(700)}$; (c)(C) $Ni/Al_2O_{3(900)}$.

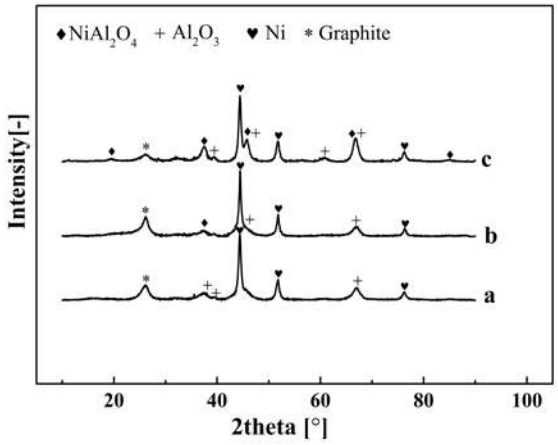

Figure 7. XRD patterns over samples after DRM in Table 3: (a) $Ni/Al_2O_{3(350)}$; (b) $Ni/Al_2O_{3(700)}$; (c) $Ni/Al_2O_{3(900)}$.

transform into C_γ with time. This may explain the absence of amorphous carbon C_α in the DTA curves of all three samples that were subjected to 100 h DRM.

Figure 8 shows TEM images of the morphologies of deposited carbon on the spent catalysts. Filament carbon with a multi-wall carbon nanotube (MWCNT) morphology was present on all three samples. Only $Ni/Al_2O_{3(350)}$ additionally featured carbon nano onions (CNO), whereby Ni particles were encapsulated within graphite carbon in Figure 8(a). The MWCNT morphology displayed different structural properties: chain-like (with or without embedded Ni particles) (Figure 8(B) or (c)), close end (Figure 8(C)), and open mouth (with or without Ni particles on the tip of the nanotube) (Figure 8(A) or (b)).

Figure 9 summarizes the different morphologies of carbon deposited on the three catalysts that originated from variations in the nature of the metal–support interaction. The coking process in DRM is believed to proceed in three steps: carbon deposition on Ni particles, carbon diffusion through the bulk Ni particles, and carbon precipitation. Besides the metal– support interaction, the coke morphology is very likely directly related to the balance between the carbon deposition and carbon diffusion–precipitation rates. Regarding $Ni/Al_2O_{3(350)}$, Ni particles from the bulk NiO sinter into larger Ni particles (40 nm) onto which the carbon deposition rate is relatively higher than the diffusion–graphite formation rate, resulting in rapid encapsulation of Ni particles into graphite carbon to form CNO, consequently leading to complete catalyst deactivation. For the Ni reduced from highly dispersed NiO, with a relatively strong interaction with the alumina support, comparable carbon deposition and diffusion–precipitation rates are expected. In this case, the deposited carbon would follow the tip–growth model: the carbon initially deposits on the top surface of the Ni metal, carbon diffuses down through the metal, and MWCNTs precipitate at the bottom of the Ni metal, driving the entire metal particle off

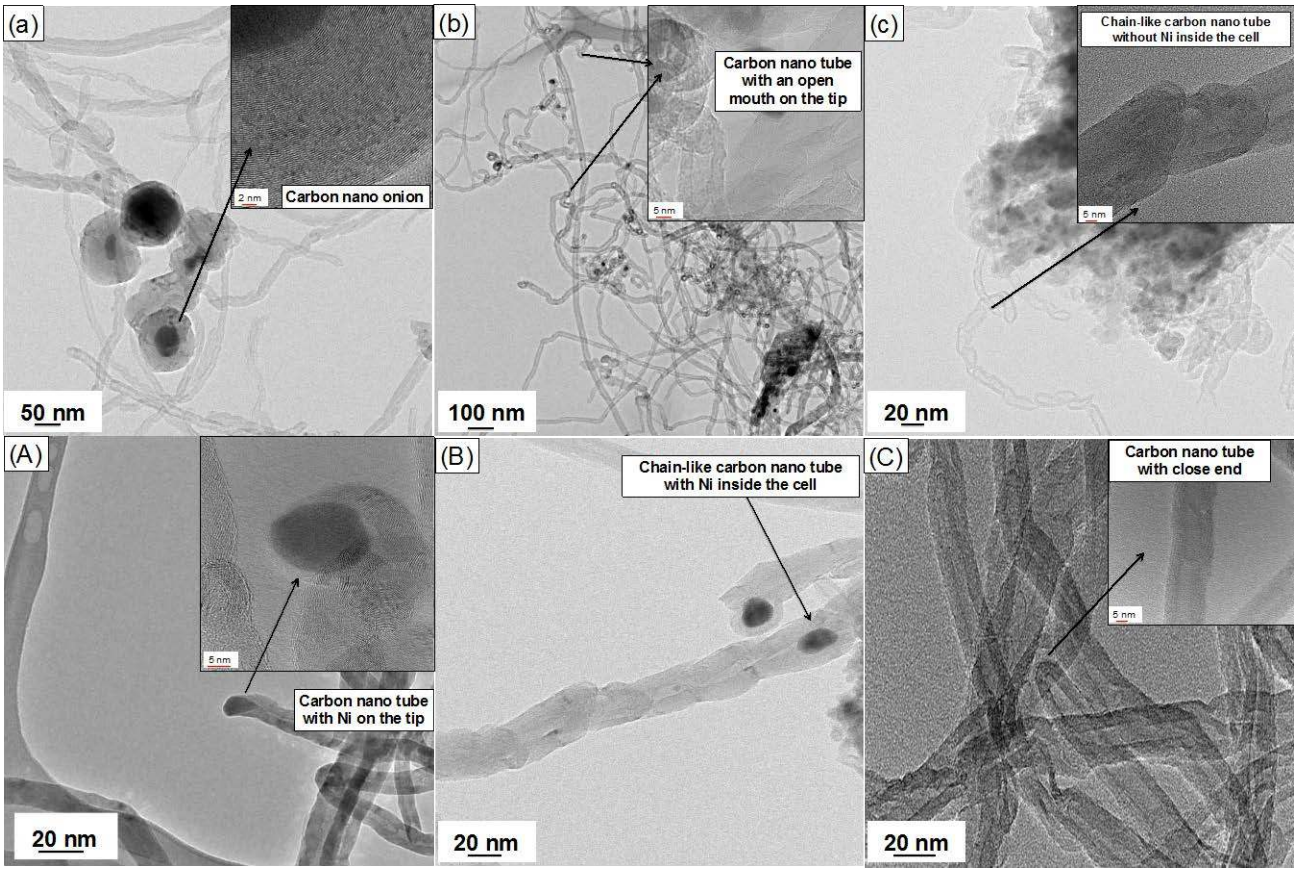

Figure 8. Different carbon deposition over the catalysts after DRM in Table 3: (a)(A) $Ni/Al_2O_{3(350)}$; (b)(B) $Ni/Al_2O_{3(700)}$; (c)(C) $Ni/Al_2O_{3(900)}$.

the support. The Ni on the tip of the MWCNTs is accessible and acts as an active site for carbon deposition. The presence of a concentration gradient in Ni promotes carbon diffusion and continual growth of the MWCNTs.

Regarding $Ni/Al_2O_{3(900)}$, the Ni–support interaction is relatively high, with an obtuse contact angle between Ni and the support. Initial carbon deposition and carbon diffusion proceed similarly to that in the tip–growth mechanism; however, the MWCNT precipitation fails to drive the Ni metal particles upwards. Hence, precipitation is forced to occur at the Ni apex, thus resulting in carbon precipitation on the other side of the exposed surface of the Ni particles rather than at the interface between the lower portion of Ni and support. This would lead to the formation of carbon nanotubes on the surface of Ni particle at the gas–solid interface. As a result, the Ni particles would be fixed on the support, but with the carbon tube growing with a closed end with Ni at the bottom of the nanotube. This is referred to as the base–growth model. Furthermore, Lee and Park[25] used this model to rationalize the formation of chain-like MWCNTs, whereby the compartment graphite sheets grew by forming joints with the wall. Because Ni from $NiO{\cdot}Al_2O_3$ in Ni-b may not have adequately strong interaction with the support, during DRM at 700°C, the Ni particles behave as a quasi-liquid and can be easily split into smaller particles and absorbed into the interior of the chain-like MWCNTs. Similar results were also reported by Hua and Wang.[26]

In all, the carbon deposition happened over all three catalysts and this explained the initial catalyst deactivation. However, the strong metal-support interaction would not only help to fix the Ni particles into the support to supress them towards sintering, but also favour the carbon tube growing with an active Ni at the bottom of the nanotube.

Conclusions

In this study, three types of alumina-supported Ni catalysts were prepared by the incipient impregnation method. The influence of calcination temperature during the catalyst preparation process on the catalyst physical structure, Ni dispersion, DRM activity, and carbon deposition was fully investigated. The findings are summarized as follows:

1. Catalysts prepared at low calcination temperatures showed high initial DRM activities, but poor stability. Ni reduced from $NiAl_2O_4$ showed better resistance to sintering and coking during DRM. It is likely that incomplete reduction of $NiAl_2O_4$ produces Ni sites that interact strongly with the support. It is believed that this strong interaction plays an important role in stabilizing the catalytic activity of Ni during DRM.
2. Carbon growth models were proposed to rationalize the different carbon morphologies observed on the three catalysts. Ni from bulk NiO is believed to sinter into larger Ni particles during DRM that were encapsulated by graphite carbon to form carbon nano onions. Based on the tip–growth and base–growth models, strong interaction between Ni and the support favors the formation of filament carbon including chain-like structures and MWCNTs with Ni on the tip.

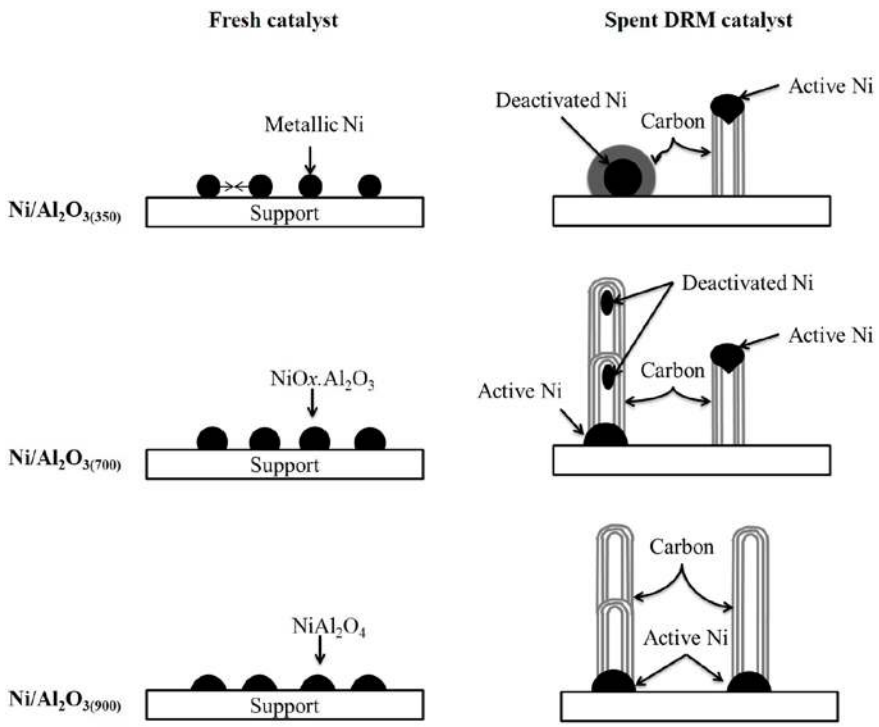

Figure 9. Image of different carbon deposition over three catalysts during DRM.

Experimental Section

Catalyst preparation

The alumina-supported Ni catalysts were prepared by incipient impregnation using $Ni(NO_3)_2 \cdot 6H_2O$ solution. Al_2O_3 (AEROXIDE® Alu 130; Brunauer–Emmett–Teller (BET) surface area of 130 m^2/g) was used as a support. The Ni loading was controlled at 16 wt.%. After impregnation, the supported Ni samples were dried at 110°C overnight and then calcined in air at 350, 700, or 900°C for 5 h. The resulting Ni catalysts are respectively referred to as $Ni/Al_2O_{3(350)}$, $Ni/Al_2O_{3(700)}$, and $Ni/Al_2O_{3(900)}$.

Catalyst characterization

The elemental composition of the samples dissolved in H_2SO_4/HNO_3 was determined by inductively coupled plasma atomic emission spectroscopy (ICP–AES) on a Thermo-Electron 3580 instrument.

N_2 adsorption–desorption isotherms were obtained on a Micromeritics ASAP2420. Prior to measurements, the samples were degassed for 2 h at 300°C. The surface areas of the samples were determined by a multi-point BET analysis method, and pore volumes were estimated at $P/P_0 = 0.99$.

XRD patterns were recorded on a Bruker D8 Advanced A25 diffractometer using a Bragg–Brentano geometry with a copper tube operating at 40 kV and 40 mA. The catalyst powder was compacted into disks and mounted in the chamber. The mean crystallite size of nickel was calculated using the Scherrer equation.

H_2-TPR was performed on an Altamira instrument. The catalyst powder (50 mg) was placed in a U-shaped quartz reactor and pre-treated in flowing Ar (50 mL/min) for 0.5 h at 300°C, followed by cooling to room temperature. The temperature was then raised from room temperature to 1000°C at a rate of 10°C/min under a 5% H_2/Ar flow (50 mL/min). A thermal conductivity detector (TCD) was employed to monitor the H_2 consumption.

Combined H_2-TPR and TPD measurements were conducted to analyse the dispersion of the Ni particles. Following TPR measurements from room temperature to 800°C, followed by isothermal heating at 800°C for 1 h, the sample was cooled to room temperature in 5% H_2/Ar mixture and allowed to stand for 1 h. The sample was then purged with pure Ar (50 mL/min) to remove the physically adsorbed H_2. Upon stability of the TCD baseline, the sample was heated at a rate of 10°C/min to 800°C in pure Ar (50 mL/min) to perform H_2-TPD measurements. The ratio of 2 × (TPD signal area)/(TPR signal area) enabled estimation of the dispersion of reduced nickel.

The catalyst reduction degree was evaluated using TGA–DTA (differential thermal analysis) (NETZSCH STA 449 F1 Jupiter). The catalyst powder (20 mg) was placed in an alumina crucible and pretreated in flowing Ar (50 mL/min) for 0.5 h at 300°C, followed by cooling to room temperature. The temperature was then raised from room temperature to 1000°C at a rate of 10°C/min under a 5% H_2/Ar flow (50 mL/min). The sample remained heated at 1000°C for a time period until no weight change was detected. The catalyst reduction degree at different temperatures was calculated by the ratio of weight loss at that temperature to the total weight loss.

The amount of carbon deposited on the catalyst was also analyzed using TGA–DTA. The spent catalyst powder (20 mg) was placed in an alumina crucible and pretreated in flowing Ar (50 mL/min) for 0.5 h at 300°C, followed by cooling to room temperature. The temperature was then raised from room temperature to 1000°C at a rate of 10°C/min under air flow (50 mL/min). The sample remained heated at 1000°C for a time period until no weight change was detected. The deposited carbon amount was calculated based on the weight loss.

TEM images were taken on a Titan G2 transmission electron microscope (FEI, Hillsboro, OR, USA), operating at 80–300 kV and equipped with a 4 k × 4 k charge-coupled device (CCD) camera (US4000) and an energy filter (GIF Tridiem, Gatan Inc., Pleasanton, CA, USA). The specimens were prepared by ultrasonically suspending the sample in ethanol. A drop of the suspension was then applied onto clean holy copper grids and dried in air.

Activity evaluation

Activity measurements of the DRM process were conducted in a PID micro-activity reactor equipped with a long quartz tube reactor (internal diameter: 4 mm; length: 305 mm), which was heated by an electrical furnace under atmospheric pressure. First, 20 mg of catalyst (size: 250–300 µm) was loaded into the reactor, and the reaction temperature was controlled by a thermocouple placed in the center of the catalyst layer. Conversions of CH_4 and CO_2 were typically adjusted to be significantly lower than those defined by thermodynamic equilibrium by adjusting the total flow rate (160 mL/min). Rate limitation by external and/or internal mass transfer under different conditions proved to be negligible under suitable experimental criteria. The feed composition of $N_2/CH_4/CO_2$ was 2:1:1 over a temperature range of 500–800°C. A pre-reduction treatment was performed by heating the catalyst at 800°C for 1 h in pure H_2 atmosphere. The outlet gases were analysed by online gas chromatography (GC; Varian 450) and micro GC (Soprane MicroGC 3000). The DRM catalyst activity was determined by evaluating both the turnover frequency (TOF) of CH_4 and CO_2. The TOF was calculated by normalizing the reaction rates to the number of exposed surface Ni atoms. The apparent activation energy (E_a) was calculated from the Arrhenius plots of the TOF.

Carbon deposition study

Thermogravimetric analyses of carbon deposits were performed on a TGA-DTA analyser under a CO_2/CH_4 (1:1) atmosphere. A 10-mg catalyst with a particle size of 250–300 µm was loaded

into an alumina crucible. The catalyst was reduced in pure H_2 for 1 h at 800°C until no further weight change was detected. The temperature was then decreased to the reaction temperature for isothermal reaction studies under a CO_2+CH_4 flow of 40 mL/min. The rate of carbon formation was obtained from the slope of the curve at the early reaction stage (<2 min). Therefore, rates of coking obtained can be regarded as the initial rates. These values were accordingly used to calculate the E_a of coking on the different catalysts studied.

Keywords: methane • dry reforming • nickel • spinel • carbon deposition

[1] D. Baudouin, K. C. Szeto, P. Laurent, A. De Mallmann, B. Fenet, L. Veyre, U. Rodemerck, C. Copéret, C. Thieuleux, *Journal of the American Chemical Society* **2012**, *134*, 20624-20627.
[2] S. H. Zhang, S. Muratsugu, N. Ishiguro, M. Tada, *Acs Catal* **2013**, *3*, 1855-1864.
[3] C. J. Liu, J. Y. Ye, J. J. Jiang, Y. X. Pan, *Chemcatchem* **2011**, *3*, 529-541.
[4] S. B. Wang, G. Q. Lu, *Industrial & Engineering Chemistry Research* **1999**, *38*, 2615-2625.
[5] M. S. Fan, A. Z. Abdullah, S. Bhatia, *Chemsuschem* **2011**, *4*, 1643-1653.
[6] S. R. de Miguel, I. M. J. Vilella, S. P. Maina, D. S. Jose-Alonso, M. C. Roman-Martinez, M. J. Illan-Gomez, *Appl Catal a-Gen* **2012**, *435*, 10-18.
[7] J. R. H. Ross, *Catal Today* **2005**, *100*, 151-158.
[8] X. Hengyong, S. Xixian, F. Yemei, X. Guolin, L. Jinxiang, Y. Wenge, Z. Peiheng, *Petrochemical Technology* **1992**, *3*, 001.
[9] A. M. Gadalla, B. Bower, *Chem Eng Sci* **1988**, *43*, 3049-3062.
[10] M. Garcia-Dieguez, I. S. Pieta, M. C. Herrera, M. A. Larrubia, L. J. Alemany, *Appl Catal a-Gen* **2010**, *377*, 191-199.
[11] L. D. Li, L. Zhou, S. Ould-Chikh, D. H. Anjum, M. B. Kanoun, J. Scaranto, M. N. Hedhili, S. Khalid, P. V. Laveille, L. D'Souza, A. Clo, J. M. Basset, *Chemcatchem* **2015**, *7*, 819-829.
[12] B. C. Enger, R. Lodeng, J. Walmsley, A. Holmen, *Appl Catal a-Gen* **2010**, *383*, 119-127.
[13] N. F. P. Ribeiro, R. C. R. Neto, S. F. Moya, M. M. V. M. Souza, M. Schmal, *Int J Hydrogen Energ* **2010**, *35*, 11725-11732.
[14] L. Zhou, Y. Guo, M. Sakurai, H. Kameyama, *Appl Catal a-Gen* **2009**, *364*, 101-107.
[15] Y. G. Chen, J. Ren, *Catalysis Letters* **1994**, *29*, 39-48.
[16] A. Nandini, K. K. Pant, S. C. Dhingra, *Appl Catal a-Gen* **2006**, *308*, 119-127.
[17] Y.-H. Wang, H.-M. Liu, B.-Q. Xu, *Journal of Molecular Catalysis A: Chemical* **2009**, *299*, 44-52.
[18] T. Osaki, T. Horiuchi, K. Suzuki, T. Mori, *J Chem Soc Faraday T* **1996**, *92*, 1627-1631.
[19] J. J. Guo, H. Lou, H. Zhao, D. F. Chai, X. M. Zheng, *Appl Catal a-Gen* **2004**, *273*, 75-82.
[20] V. A. Tsipouriari, X. E. Verykios, *Catal Today* **2001**, *64*, 83-90.
[21] Y. H. Hu, E. Ruckenstein, *Catalysis Reviews* **2002**, *44*, 423-453.
[22] J. Juan-Juan, M. Roman-Martinez, M. Illan-Gomez, *Applied Catalysis A: General* **2009**, *355*, 27-32.
[23] J. Guo, H. Lou, X. M. Zheng, *Carbon* **2007**, *45*, 1314-1321.
[24] M. D. Argyle, C. H. Bartholomew, *Catalysts* **2015**, *5*, 145-269.
[25] C. J. Lee, J. Park, *Appl Phys Lett* **2000**, *77*, 3397-3399.
[26] A. C. Lua, H. Y. Wang, *Appl Catal B-Environ* **2013**, *132*, 469-478.

FULL PAPER

The Ni reduced from $NiAl_2O_4$ showed an excellent performance against sintering and coking during a long-term methane dry reforming reaction.

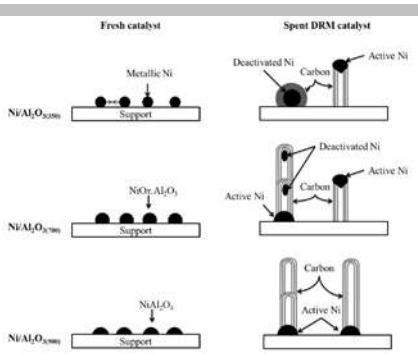

*Lu Zhou, Lidong Li, Nini Wei, Jun Li, Kazuhiro Takanabe and Jean-Marie Basset**

Page No. – Page No.

Effect of $NiAl_2O_4$ formation on Ni/Al_2O_3 Stability during Dry Reforming of Methane